Sea Surface Emissivity Observations at L-Band: First Results of the Wind and Salinity Experiment WISE 2000

A. Camps, *Member, IEEE*, J. Font, J. Etcheto, V. Caselles, A. Weill, I. Corbella, *Member, IEEE*, M. Vall-llossera, N. Duffo, *Member, IEEE*, F. Torres, R. Villarino, L. Enrique, A. Julià, C. Gabarró, J. Boutin, *Associate Member, IEEE*, E. Rubio, S. C. Reising, *Member, IEEE*, P. Wursteisen, M. Berger, and M. Martín-Neira, *Member, IEEE*

***Abstract*—Sea surface salinity can be measured by passive microwave remote sensing at L-band. In May 1999, the European Space Agency (ESA) selected the Soil Moisture and Ocean Salinity (SMOS) Earth Explorer Opportunity Mission to provide global coverage of soil moisture and ocean salinity. To determine the effect of wind on the sea surface emissivity, ESA sponsored the Wind and Salinity Experiment (WISE 2000). This paper describes the field campaign, the measurements acquired with emphasis in the radiometric measurements at L-band, their comparison with numerical models, and the implications for the remote sensing of sea salinity.**

***Index Terms*—Emissivity, microwave radiometry, sea measurements, sea surface electromagnetic emission.**

I. Introduction

SEA SURFACE salinity can be measured by passive microwave remote sensing at L-band, where there is a reserved frequency band (1.400–1.427 MHz): this frequency is a compromise between the sensitivity of the brightness temperature to the salinity, small atmospheric perturbation, and reasonable pixel resolution [1]. To provide soil moisture and ocean surface salinity global coverage measurements with three-day revisit time, the European Space Agency (ESA) selected in May 1999 the Soil Moisture and Ocean Salinity (SMOS) Earth Explorer Opportunity Mission [2], [3]. SMOS will be the first two-dimensional (2-D) synthetic aperture radiometer for earth observation. The scanning configuration of SMOS presents new challenges:

1) 2-D imaging of the scene, with varying incidence angles and pixel resolution as the pixel travels through the alias-free field of view;
2) polarization mixing between vertical and horizontal polarizations due to the relative orientation between the antenna reference frame and the pixel's local reference frame;
3) not yet well-understood azimuthal dependence of the first two Stokes parameters (T_v and T_h) with wind direction;
4) unknown signature of the third and fourth (U and V) Stokes parameters and their azimuth/elevation dependence with wind speed (WS);
5) effect of sea foam at L-band.

The WISE 2000 campaign was sponsored by ESA to collect experimental data under the widest possible range of wind conditions to better understand the polarimetric emission at L-band of the sea surface and its dependence with wind and salinity [points 1), 3), and 4)]. Point 2) is a known geometrical problem, and point 3) is being addressed specifically by the ESA-sponsored L-Band Ocean Salinity Airborne Campaign (LOSAC).

The WISE 2000 campaign took place at the Casablanca oil rig, located at 40° 43.02′ N 1° 21.50′ E, 40 km away from the Ebro River mouth at the coast of Tarragona (Spain). The sea conditions are representative of the Mediterranean shelf/slope region with periodic influence of the Ebro River fresh water plume. Systematic measurements were acquired from November 16 to December 18, 2000, and continued during January 9–15, 2001. The WISE 2000 participants have been

1) Polytechnic University of Catalonia (UPC, Barcelona, Spain, prime contractor);
2) Institut of Marine Sciences (ICM-CSIC, Barcelona, Spain);
3) Laboratoire d'Océanographie Dynamique et Climatologie (LODYC, Paris, France);
4) University of València (UV, València, Spain);
5) Centre d'Études Terrestres et Planétaires (CETP, Paris, France);
6) University of Massachusetts–Amherst (UMass, USA) as a guest institution.

The instruments that were deployed were as follows:

- L-band polarimetric radiometer [UPC, Fig. 1(a)];
- Ka-band polarimetric radiometer [UMass, Fig. 1(b)];

Manuscript received September 20, 2001; revised March 9, 2001. The WISE 2000 campaign was supported by the European Space Agency under ESTEC Contract 14188/00/NL/DC. The numerical simulations have been performed under ESTEC Salinity Study 3618. The implementation of the L-band radiometer of the Polytechnic University of Catalonia has been supported by the Spanish government under Grant CICYT TIC99-1050-C03-01. The French moorings were supported by the Centre National d'Études Spatiales.

A. Camps, I. Corbella, M. Vall-llossera, N. Duffo, F. Torres, R. Villarino, and L. Enrique are with the Department of Signal Theory and Communications, Universitat Politècnica de Catalunya, 08034 Barcelona, Spain (e-mail: camps@tsc.upc.es).

J. Font, A. Julià, and C. Gabarró are with the Institut de Ciències del Mar, CMIMA-CSIC, 08003 Barcelona, Spain.

J. Etcheto and J. Boutin are with the LODYC, UPMC, 75252 Paris Cedex 05, France.

V. Caselles and E. Rubio are with the Departament de Termodinàmica, Facultat de Física, 46100 Burjassot, Valencia, Spain.

A. Weill is with the CETP, 78140 Vélizy, France.

S. C. Reising is with the Microwave Remote Sensing Laboratory, University of Massachusetts, Amherst, MA 01003 USA.

P. Wursteisen, M. Berger, and M. Martín-Neira are with the European Space Agency, ESTEC, 2200-AG Noordwijk, The Netherlands.

Digital Object Identifier 10.1109/TGRS.2002.802496

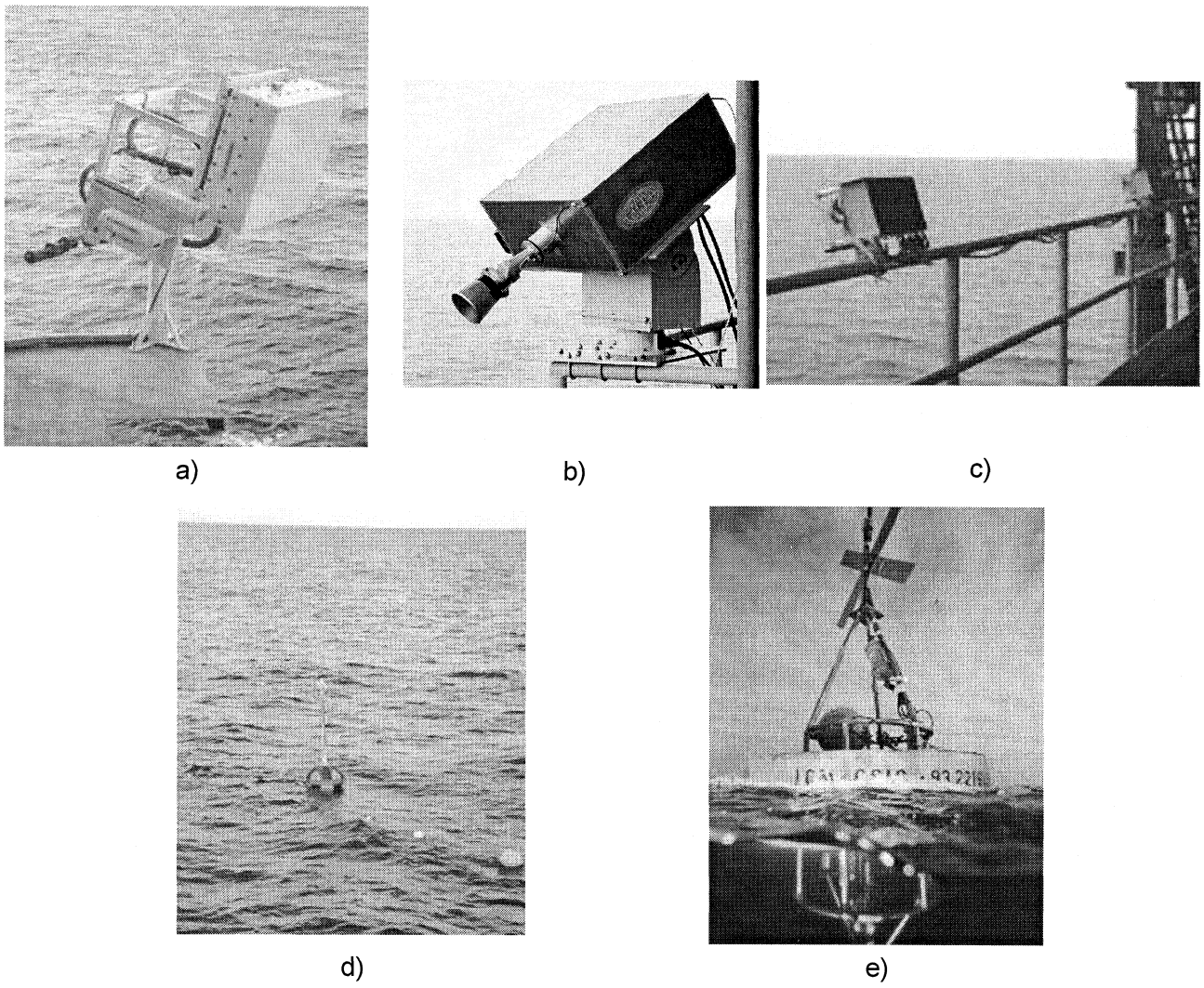

Fig. 1. Instrumentation deployed during WISE 2000. (a) L-band polarimetric radiometric (UPC), video camera (UPC), and IR radiometer IR (UV), b) Ka-band polarimetric radiometer (UMass), (c) stereocameras (CETP), (d) buoy 2 (ICM-CSIC and LODYC), (e) buoy 1 for accurate SSS and SST measurements (ICM-CSIC).

- stereo-camera to determine surface topography and rms slopes of the sea surface [CETP, Fig. 1(c)];
- three oceanographic and climatologic buoys for near-surface salinity, temperature, wind speed and direction, wave height and period, etc. [ICM-CSIC and LODYC, Fig. 1(d) and (e)];
- portable meteorological station with atmospheric pressure, air temperature, relative humidity, and rain rate (UPC);
- video camera mounted on the L-band radiometer pedestal to determine sea surface foam coverage[1] [UPC, Fig. 1(a)];
- Infrared (IR) radiometer to determine sea surface temperature (SST) estimates [UV, Fig. 1(a)].

The relative orientation of each instrument is shown in Fig. 2. Additionally, temperature and salinity were recorded from the platform at 5 m below the sea level, and ocean color, wind vector, and SST satellite imagery were acquired.

[1]Video camera field of view $25^\circ \times 32^\circ$ selected to match as close as possible the L-band antenna half-power beam-width (20°). During the video processing, a mask was applied to each photogram to select a circular field of view of 20°.

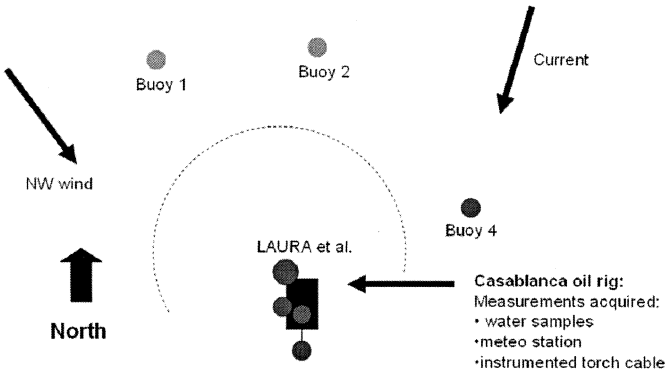

Fig. 2. Sensor locations during WISE 2000 around the Casablanca oil rig.

II. Analysis of *In Situ* Data

A. Sea Surface Temperature and Salinity

Sea surface temperature and salinity in the area of the Casablanca oil rig were monitored by means of *in situ* sensors deployed in moored buoys. Since neither buoy 1 nor buoy 4

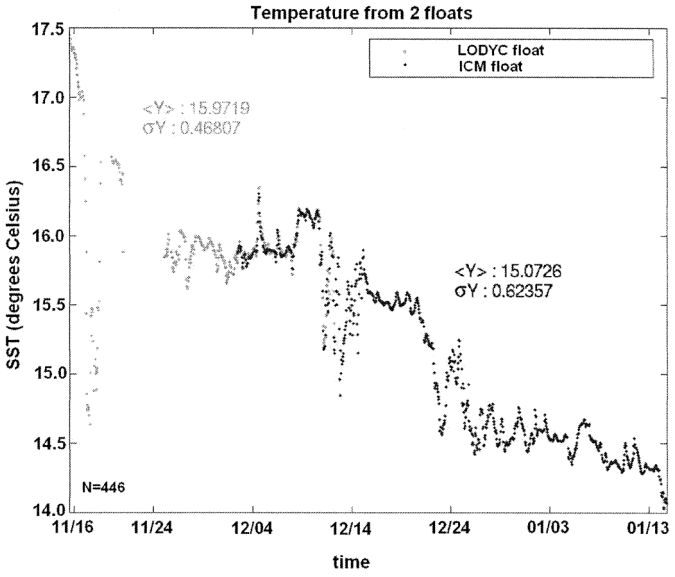

Fig. 3. SST (degrees Celsius) evolution during WISE 2000 (dark gray: buoy 1, light gray: buoy 4).

worked for the whole duration of the campaign, their measurements for the common period were compared for the common period, and a complete series of data was reconstructed.

The surface temperature temporal evolution (Fig. 3) is typical of the autumn season. During the first two weeks of WISE 2000, the temperature decreased by more than 1.5 °C; then the surface cooling continued regularly for the rest of the measurement period, with another strong drop around December 20, and even some short periods of small increase around December 10. In total, SST ranged from 17.5 °C to 14 °C.

Fig. 4 shows the evolution of the sea surface salinity (SSS). During the whole experiment period, it remained near 38 psu, a value typical of the Mediterranean open sea waters that, unlike temperature, does not display a clear seasonal salinity signal. This means that the WISE area was usually out of the direct influence of the Ebro River discharge. The salinity time series shows the occurrence of some low SSS events that typically had a duration of 5–6 days. These events, especially the one around December 12 (strongest SSS drop), are associated with similar SST decreases, a possible indication of the river plume reaching the Casablanca area, as continental waters are not only fresher, but also colder than ambient water. This interpretation has been confirmed by the sequence of satellite Advanced Very High Resolution Radiometer (AVHRR) IR images that display the evolution of the cold-water tongue from the river mouth to this offshore location. The standard situation presents an along-slope current from the northeast that keeps the river plume close to shore and continental waters flowing to the southwest, away from the platform. Occasionally, current reversals, strong southerly winds, or a significant increase of the river discharge allow these lower salinity waters to reach the experiment area. The two main events detected during WISE resulted in recorded SSS values 2 psu (December 12) and almost 1 psu (December 25) lower than the regular 37.9–38 psu observed all around the experiment.

An important issue related to salinity remote sensing is the possible presence of a vertical salinity gradient. A microwave radiometer will only measure the very surface values ($\sim$ 1 cm), which is not the case of *in situ* sampling, where sensors have to be completely immersed in sea water. Validation of SMOS salinity determinations will strongly rely on *in situ* measurements made from standard moored or drifting buoys, or even hydrographic casts or underway measurements from research or opportunity vessels. In all these cases, temperature, and especially conductivity, sensors are not operated close to the surface to avoid interference from air bubbles and even to protect them from possible sources of dirt. A present standard value for near-surface salinity measurement is 5 m below sea level. In some cases, especially after strong rainfall, salinity at this depth can be significantly different from SSS, and then, errors can be introduced by comparing both values.

The difference between salinity close to the surface (-20 cm, buoy 1) and at -5 m was monitored during WISE 2000 by deploying a second instrument from the platform at this depth. Most of the time, the difference between both time series is below 0.1 psu, a value that can be considered a threshold for SSS satellite remote sensing resolution. It is only noticeable during the reported low-salinity events, especially that of December 10–15 when the difference reached up to 2.0 psu. (This observation is another confirmation that this event was due to an intrusion of the river plume, a near-surface phenomenon, since at -20 cm the salinity drop from ambient water was almost 2.1 psu, while at -5 m it was only 0.5 psu maximum.) This poses an additional problem to the satellite SSS validation that has to be analyzed in the framework of the general calibration/validation strategy and considering the decorrelation scales at open oceans.

B. Analysis of Wind Speed Data

Wind speed data from three different sources was acquired:

- meteorological station at 69-m height on the Casablanca oil rig every 15 min;
- buoy 2 provided a measurement at 2.6-m height every 2 min;
- satellite-borne scatterometer (QUIKSCAT).

The first step is to map the *in situ* measurements to 10-m height (meteorological standard), assuming neutral stability. In order to check this hypothesis, the ratio of the wind speed measured by the two instruments was plotted versus the air temperature minus the water temperature. No tendency is visible in Fig. 6, even though the water is on average 1° warmer than the air, indicating an atmosphere that is generally slightly unstable.

The platform meteorological station was the only instrument that measured for the whole period. The measurements of the three instruments mapped to 10-m height are plotted versus time in Fig. 7. The wind speed averaged during the whole period is 6.8 m/s. Wind speeds higher than 15 m/s were observed on November 17, 24, and 26, on December 15, 28, 29, 30, and 31, and on January 5, 6, and 8. Unfortunately, the strongest winds were observed during the period around December 25–January 1, during which the manned experiments were not operated.

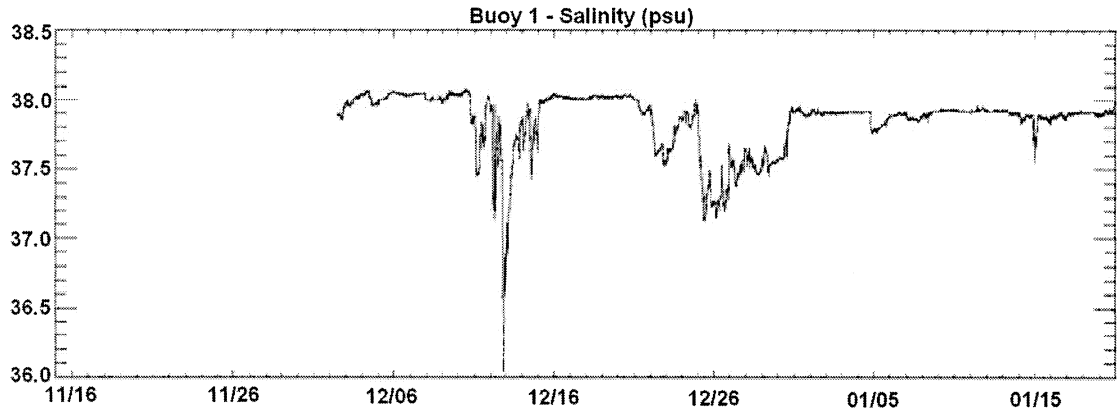

Fig. 4. SSS (psu) evolution during WISE 2000.

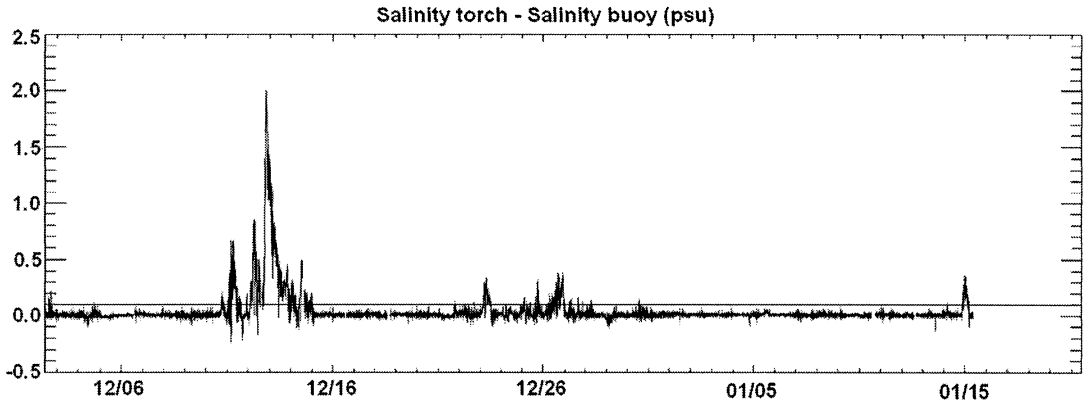

Fig. 5. Salinity difference between sensors located at -5 m and -0.2 m.

The measurements made by the different instruments were mapped to 10-m height during the period of common measurements and were averaged during one hour. The regression line of the measurements of the meteorological station on the platform (y axis) against the measurements made simultaneously by buoy 2 in the range 3–15 m/s (most commonly observed wind speed range and optimal range for instruments) and in the whole data range is $U_M = 1.09U_B + 0.07$ with an explained variance of 92%; in the whole range, it is $U_M = 1.17U_B - 0.20$ with an explained variance of 96%. The mean difference between the instruments is $\langle U_B - U_M \rangle = -0.92$ m/s with a standard deviation of 1.83 m/s. In the most commonly observed range, the instruments differ by about 10%, the standard deviation of the difference being rather high. The measurements are nevertheless usable for checking emissivity models. This discrepancy might be due to several factors: different instruments, different height (the mapping to 10 m is not perfect; from 69 m it is a large correction, and atmospheric stability correction did not improve the result), and the platform is likely to disturb the air flow less at the top than at low altitude. However, it must be noticed that if the 69-m height is assumed to be relatively free from the platform disturbance, it is not in the surface layer from which the 10-m wind speed (U_{10}) can be computed from "universal parametrizations." Therefore, a special algorithm was devised to take into account this effect. Inside the boundary layer the Smith *et al.* [4] drag coefficient is used. For the measurements made at 69-m height, it was assumed that the boundary layer thickness was ten times the value of U_{10} and that the wind speed was independent of height in the mixed layer. First, U_{10} was computed from U_{69}, assuming that the measurement was made in the boundary layer. If $10U_{10}$ was smaller than 69 m, it was assumed that the boundary layer thickness was $10U_{10}$, and the process was repeated until it converged.

Measurements of the QUIKSCAT scatterometer (nudge algorithm) were colocated with the platform using a radius of 0.27° latitude and 0.37° longitude: 196 measurements were found for the duration of the campaign. Since the scatterometer cannot approach closer than 50 km from the coast, no measurement was coincident with the platform: all of them were east and south. These data were averaged for each satellite pass, and the resulting average was compared with one-hour average of the *in situ* measurements. The scatter plot of QUIKSCAT data versus the meteorological station measurements at 10-m height that is fit in the range 3–15 m/s is $U_Q = 0.97U_M + 0.68$ with an explained variance of 74%; the mean difference between the instruments $\langle U_M - U_Q \rangle$ is 0.44 m/s with a standard deviation of 2.8 m/s. Even though the points are rather scattered, probably due to the imperfect colocation, they compare rather well.

C. Analysis of IR Radiometric Data

A CE312 IR radiometer (Table I) was installed in the L-band radiometer pedestal to derive SST estimates for comparison

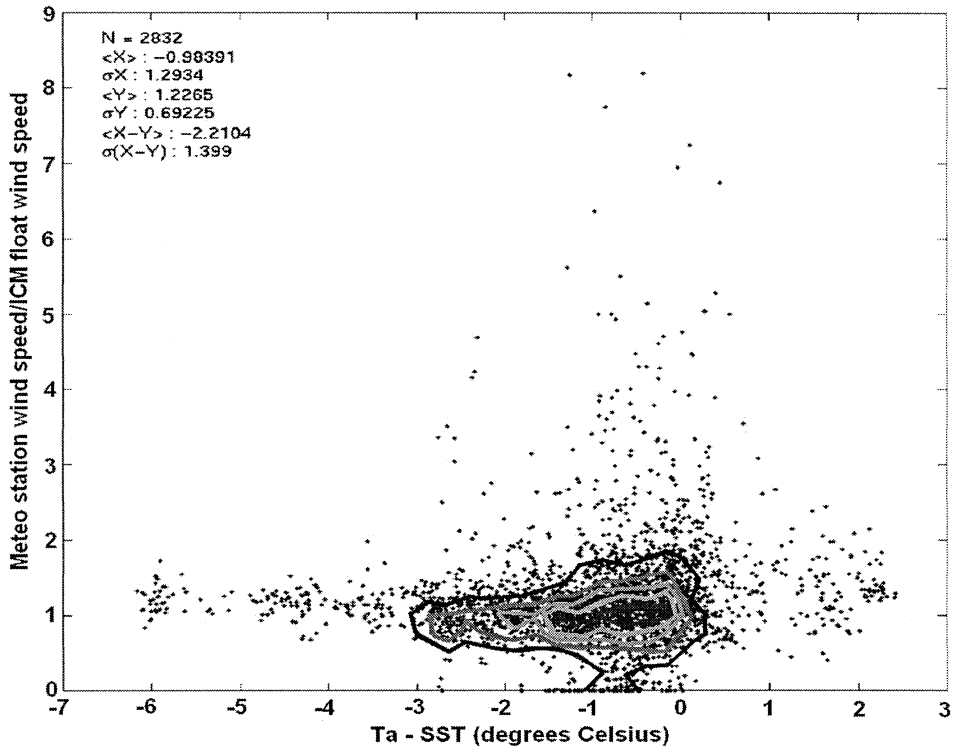

Fig. 6. Stability test. Wind speed at 10-m height ratio versus air–sea temperature difference.

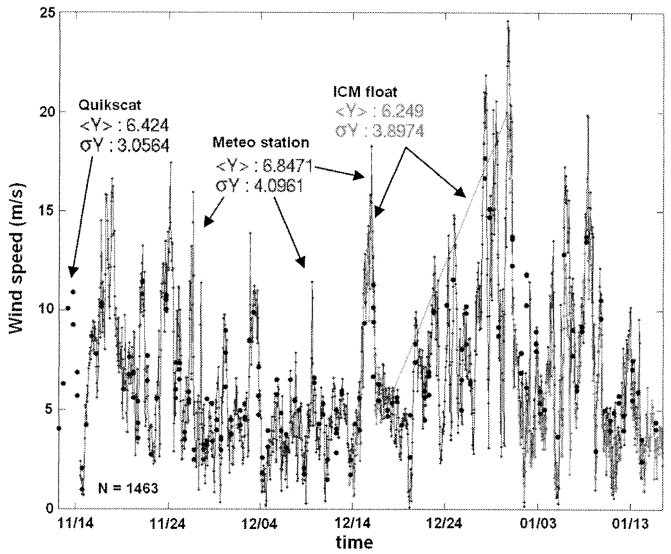

Fig. 7. Wind speed mapped at 10 m from different sources. Meteo station, buoy 2 (missing data between December 17–30) and QUIKSCAT satellite (dots).

with the thermodynamic temperature and satellite-derived SST estimates.

The radiance $R(\theta)$ reaching the sensor when looking at sea surface at an elevation angle θ is composed of three contributions: 1) the sea surface direct emission, which is attenuated by the transmittance of the atmosphere between the sea and the instrument, τ; 2) the reflection of the down-welling sky radiance ($L^{\downarrow}_{\rm sky}$) on the sea, also attenuated by the atmosphere; and 3) the upwelling atmospheric radiance emitted along the viewing direction ($L^{\uparrow}_{\rm sky}$). For clear skies, a horizontally homogeneous sky can be assumed, and $L^{\downarrow}_{\rm sky}$ depends only on the elevation angle

$$R(\theta) = \left[\varepsilon(\theta, U_{10})B(\mathrm{SST}) + (1 - \varepsilon(\theta, U_{10}))\, L^{\downarrow}_{\rm sky}(\overline{\theta_r})\right] \cdot \tau(\theta) + L^{\uparrow}_{\rm sky}(\theta) \quad (1)$$

where $B(\mathrm{SST})$ is the Planck radiance for a skin temperature SST value; ε is the emissivity of the roughened seawater; U_{10} is the surface wind speed; and $\overline{\theta_r}$ is an effective angle of incidence of the reflected radiance that is close to the viewing angle [5], [6].

In the derivation of SST estimates, the following approximations have been assumed.

1) Sea surface emissivity is derived from [7].
2) Down-welling atmospheric radiance is corrected by performing sky measurements at zenith angles equal to the sea surface incidence angles.
3) Up-welling radiance and atmospheric transmittance are corrected using MODTRAN radiative transfer software.

TABLE I
RADIOMETERS AND OBSERVATION GEOMETRY PARAMETERS

Parameter	L-band radiometer	CE312 radiometer
Frequency bandwidth/Spectral range	1405-1422 MHz	8-13 μm (channel 1)
Sensitivity	0.4 K	8 mK
Integration time	1 s	20 s
Estimated accuracy	± 1 K	±0.10 K
Observation height	32 m	32 m
Incidence angle	25°-65°	25°-65°
Angular resolution (half-power)	20°	10°
Spatial resolution at incidence angles:	12.3 x 13.6 m	6.2 – 6.8 m
25° and 65°	26.4 x 62.5 m	13.2 – 31.2 m

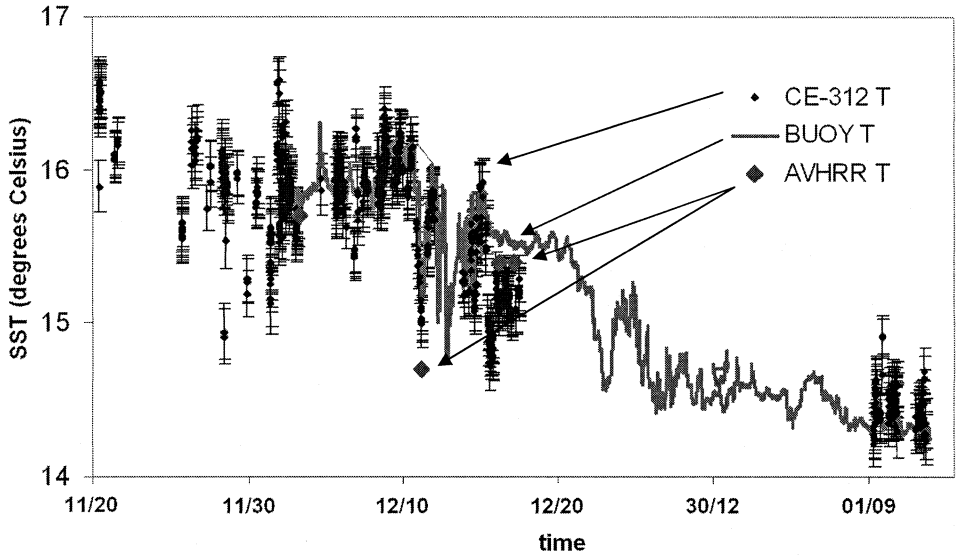

Fig. 8. Comparison between the SST observations registered by the oceanographic buoys of ICM and LODYC and those retrieved from the CE312 radiometric measurements performed in the 8–12-μm region and at 25° to 35° elevation angle.

It is found that for water vapor content, up to 5 g/cm^2 and large incidence angles (65°), biases of up to 1 K may occur in the retrieved SST when the radiometer is located at 32 m over the sea surface.

4) *Viewing geometry:* Only incidence angles of 25° and 35° have been used in the derivation of SST because of the smaller errors associated with sea surface emissivity uncertainty, reflected down-welling atmospheric radiance, and pointing errors [8].

Actual SST and its total error have been calculated from the CE312 radiometric measurements and the meteorological parameters collected from November 15 to December 23, 2000, and from January 8 to 13, 2001. SST error are generally below $\pm$0.2 K. These results have been compared with the sea temperatures registered by the oceanographic buoys and the AVHRR for four different dates (Fig. 8). The agreement of the sea temperatures in general is excellent. The differences between buoy-derived SST and CE312 SST range between 0.05–0.3 K, which are consistent with previous observations and are believed to be due to the skin effect.

Except in very high wind conditions, for the four coincident AVHRR images,[2] the average difference between the CE312-derived SST and the AVHRR observations is -0.05 K, which is negligible in relation with the uncertainty of $\pm$0.1-0.2 K of the CE312 temperatures. Therefore AVHRR-derived SST can be used as an input parameter in SSS retrieval algorithms.

D. Analysis of Sea State

The failure of buoy 3 after the first deployment attempt resulted in a lack of wave rider data. Only significant wave heights and periods, at a sampling rate of 2 min, were recorded by buoy 2 sensors. In addition to that, the reported problem on a connector in buoy 2 resulted in these wave data being only available from December 13, 2000, to the final recovery of the moorings in January 20, 2001. During these five weeks, significant wave height (computed as the average of the highest third of the waves) ranged from 0.1–4 m, with an average of near 1 m. Wave periods ranged from 1.6–7.5 s, with an average of 3.2 s.

[2]The 2-km AVHRR data was provided by the Service d'Archivage et de Traitement Météorologique des Observations Spatiales (SATMOS) data center.

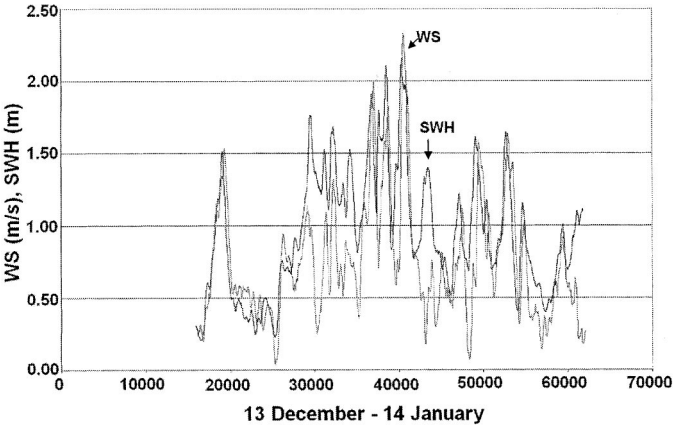

Fig. 9. Low passed (6-h filter) wave height [m] (dark gray) and wind speed [m/s] (light gray) for the period December 13 to January 14.

As it can be seen in Fig. 9, most of the time wave height is highly correlated to wind stress, which means that waves are mainly due to local wind. Hence, wind speed values can be used as a parameter for the determination of surface roughness in the sea surface emissivity numerical models. However, sometimes during the campaign, considerable wave heights were recorded without simultaneous high wind (records around 3000, 4300, and 6100 in Fig. 9), an indication that the wave field at the Casablanca site was at that moment not originated by local winds, but arrived there from external areas (swell). This is an important issue to be solved for SMOS salinity retrieval, if wind speed information has to be used in the computation.

E. Analysis of Video and Stereo-Camera Data

Two digital stereo cameras looking at the sea surface from the Casablanca oil rig were dedicated to sea surface elevation estimation and sea foam coverage. The stereo cameras pointed

to the north from a 25.8-m height and a slant angle 15.1° from the horizontal plane. Each camera has a view angle of 37.86° × 28.96°, and 832 × 624 pixels.

Approximately 3000 pairs of pictures were acquired. It was found that in the north sides the surface topography was quite complex due to the presence of swell and the reflections on the platform structure (Fig. 2), which affects the following.

- *Surface Topography:* It was observed that the spectrum in the range between a few meters to 10 m was very complex, showing the influence of reflected waves, while between 2–6 m it became more and more isotropic.
- *Total Foam Coverage:* In the north side, CETP-derived sea foam percent coverage (C_f) is

$$C_f = 1.89\ 10^{-5}\ {U_{10}}^{3.53} \tag{2}$$

where U_{10} is the wind speed in meters per second referred to 10 m. This estimate, which is rather low, corresponds to the observations made *de visu* that the wave breaking was smaller in the north side of the platform than in the west side. This can be explained by the wave reflection that prevents the incoming waves from becoming very unstable and break.

Sea foam coverage was also determined from the 19.577 video frames from the camera mounted on the radiometer antenna, which scanned from 110° west to 40° east. The UPC-derived sea foam coverage is

$$C_f = 2.32\ 10^{-4} {U_{10}}^{3.50}. \tag{3}$$

Note that the exponent of U_{10} in (3) is almost exactly the same as the one found in (2). The value of the constant is also in agreement with the results in [9], but is about an order of magnitude higher than the value found in (2) which, as discussed previously, may be due to the stabilization of the wave due to the interaction between the incoming wave and the reflected one on the north side of the platform.

III. Analysis of L-Band Radiometric Data

The UPC L-band Automatic Radiometer (LAURA) is a fully polarimetric radiometer (Table I). It has two Dicke radiometers to measure the horizontal and vertical brightness temperatures (T_h and T_v). The third[3] (U) and fourth (V) Stokes parameters are measured by means of a complex correlator. The radiometer was mounted on a terrace specially designed and built for this experiment. The terrace was located in the northwest corner at 32 m above sea level to have clear view of the zenith, and the widest possible angular excursion pointing in the upwind direction [Figs. 1(a) and 2].

The measurements were restricted in elevation from 25° incidence angle (limited by the radiometers' terrace and the Casablanca oil rig itself) to 65° (limited by the secondary lobe pointing to the horizon). In azimuth, the scan was limited to something more than 120°, from 110° west (limited by the radiometers' terrace at low incidence angles and by the safety ship at high incidence angles) to about 20° east (limited by the radiometers' terrace at low incidence angles).

The calibration procedure (from output voltages to brightness temperatures and from correlator counts to U and V) is a two-point calibration (sky: cold load; microwave absorber: hot load) for the Dicke radiometers and a correlated/uncorrelated noise injection for the correlation radiometer. The calibration procedure is described in detail in [10] and includes corrections for the following:

- atmospheric, cosmic, and galactic noise contributions scattered on the sea surface computed and subtracted from antenna temperatures;
- finite beamwidth effects;
- tilt oscillations ($< 0.2°$ rms) due to high winds.

A. Incidence Angle and Azimuth Signatures

Three types of measurements were acquired: scans in incidence angle ($\theta = 25°$ to 65°), scans in azimuth angle (five different angular positions in a 140° span), and fixed orientation to have coincident footprints with the stereo camera. Each angular position was measured during 5 min, a period in which the sea state can be considered stationary. Then, measurements (1-s integration time) at each angular position were filtered from radio-frequency interference (RFI) and averaged.

Fig. 10 presents typical measurements of elevation scans at horizontal (left) and vertical polarizations (right) for two different wind speeds: 1.3 m/s [Fig. 10(a) and (b)] and 11.9 m/s [Fig. 10(c) and (d)]. The wind speeds correspond to U_{10} averaged during the measurement interval. The trends are almost always the expected ones with two exceptions: an increase at higher incidence angles (65°, and sometimes 55°) at horizontal polarization, and a decrease at low incidence angle (25°) at vertical polarization. The increase at horizontal polarization was clearly identified as RFI coming from the coast of Tarragona and was minimized/avoided by taking most of the measurements to the west. The decrease at vertical polarization is not well understood, but it may probably be due to the metallic structure of the Casablanca platform.

Fig. 11 shows typical measurements of azimuth scans at horizontal (left) and vertical (right) polarizations for three different wind speeds and incidence angles: Fig. 11(a) and (b), $\theta = 25°$, WS = 2.7 m/s; Fig. 11(c) and (d), $\theta = 45°$, WS = 2.8 m/s; and Fig. 11(e) and (f), $\theta = 35°$, WS = 10.9 m/s. Azimuth are referred to the upwind direction. It should be noted that in most scans, there are missing points due to RFI, especially those pointing to the geographic north. Even though there are very few data points covering about one third of a full 360° scan, a small 0.1–0.2 K modulation is detected. This conclusion is not definitive and is being addressed specifically by the LOSAC campaign.[4]

In the past years, improved methods have been developed to model the polarimetric emission of the sea surface [11]–[13] and retrieved wind speed vector. However, these models have been developed or tuned at higher frequencies, typically 19 and 37 GHz. Therefore, the solid lines have been computed using a

[3]U is the third Stokes parameter, not to be confused with U_{10} or U_{69}, the wind speed referred to 10- or 69-m height.

[4]LOSAC campaign is carried out by the Technical University of Denmark, under ESA sponsorship.

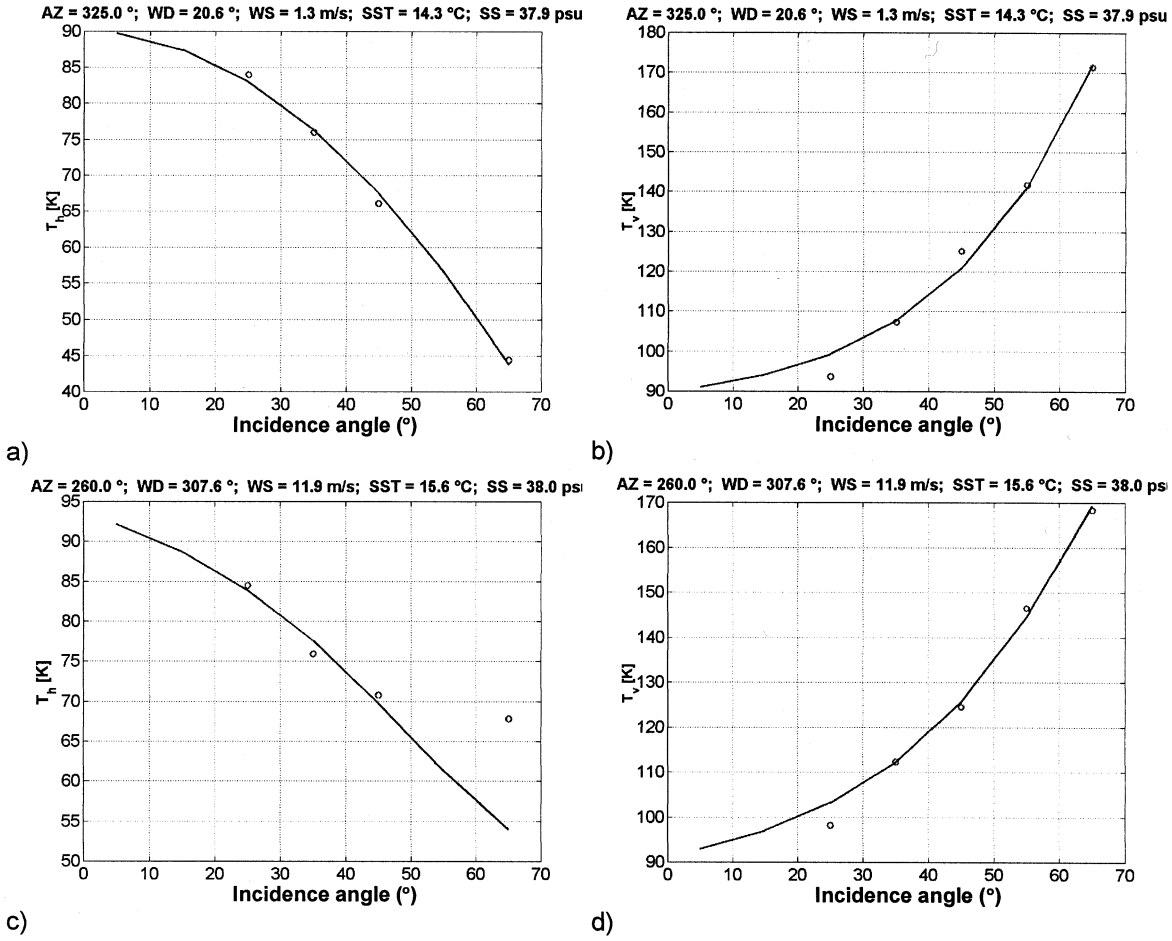

Fig. 10. Sample measurements of incidence angle scans at horizontal (left) and vertical polarizations (right) for two different wind speeds: (a) and (b) 1.3 m/s and (c) and (d) 11.9 m/s.

simple, fast, and accurate extended Kirchhoff model under the stationary phase approximation [14] that describes well the incidence angle dependence at L-band, and also the 19 and 37 GHz Jet Propulsion Laboratory measurements. The sea foam effects at L-band are hard to model. According to recent results [15], only sea foam thicker than 2 cm may produce an increase of the L-band brightness temperatures, but experimental verification is required. Therefore, instead of foam coverage models [9] linked to sea foam emissivities [16] (yet to be determined experimentally at L-band), the simple Wilheit's approximation [17] has been used. Since during WISE 2000, most of the time U_{10} was smaller than 10 m/s and the atmosphere was just slightly unstable, sea foam must have a very small or even negligible effect on the brightness temperatures, as already found in [18] and [19].

No available measurements coincident with the stereo camera are available, since it was pointing to the north, the direction from where the strongest RFI was coming.

B. Sensitivity to Wind Speed

Since the effect of wind on the brightness temperatures may mask the signature due to salinity, the determination of the sensitivity of the brightness temperatures to wind speed has been the main goal of the WISE 2000 campaign. In addition, these measurements are completely necessary to find out the best parametrization of the numerical models.

Numerical models predict a quasi-linear dependence of the brightness temperature with respect to wind speed. Only at wind speeds higher than 10 m/s approximately, foam effects may introduce a nonlinearity, indeed not yet quantified by measurements. Therefore, since during WISE 2000 most of the data were acquired under low to moderate wind conditions, a linear regression of brightness temperature data with respect to U_{10} was performed. In order to determine it, all the data files have been read, and the data points have been sorted by polarization and incidence angle. First, data points with an anomalous high value or those exceeding $\pm 4\sigma$ from the linear regression were suspected to be wrong or corrupted by RFI and were filtered out. Fig. 12 shows the L-band brightness temperature at horizontal (left) and vertical (right) polarizations at different incidence angles: Fig. 12(a) and (f) $\theta = 25°$, Fig. 12(b) and (g) $\theta = 35°$, Fig. 12(c) and (h) $\theta = 45°$, Fig. 12(d) and (i) $\theta = 55°$, and Fig. 12(e) and (j) $\theta = 65°$ plotted with respect to U_{10}. Table II lists the number of available data points for each plot. As it can be appreciated, the number is much smaller at horizontal polarization because of RFI, and decreases dramatically at higher incidence angles. This induces larger uncertainties (percentile 50 dotted lines in Fig. 12) and in the estimation of the slope.

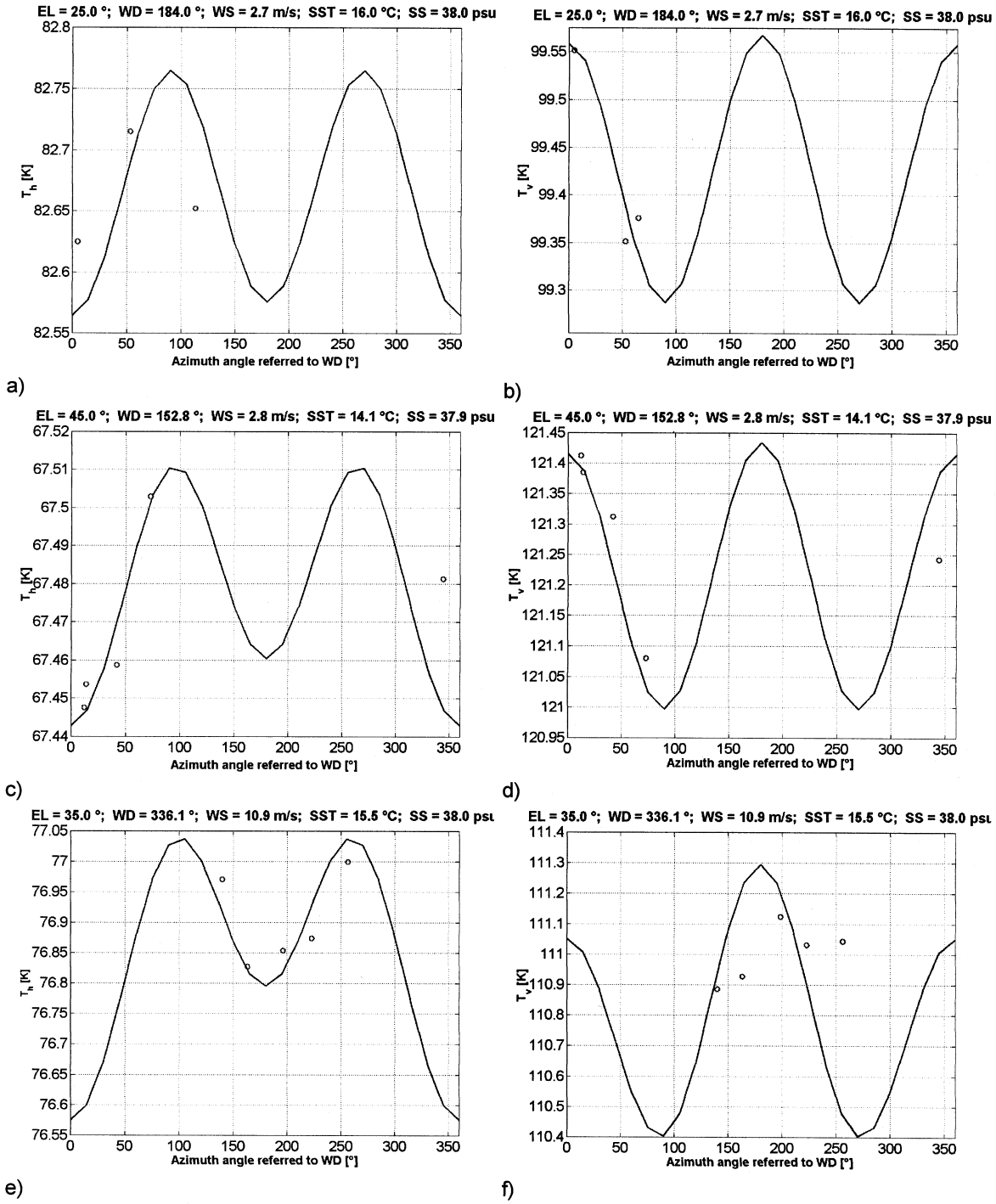

Fig. 11. Sample measurements of azimuth scans at horizontal (left) and vertical (right) polarizations for three different wind speeds and incidence angles. (a) and (b) $\theta = 25°$, WS $= 2.7$ m/s; (c) and (d) $\theta = 45°$, WS $= 2.8$ m/s; and (e) and (f) $\theta = 35°$, WS $= 10.9$ m/s.

Fig. 13 presents the estimated slopes at horizontal and vertical polarizations versus incidence angle and their associated error bars. It is found that error bars are mostly due to the uncertainty in the wind speed estimation ($\sigma_{\mathrm{WS\ meteo-WS\ buoy}} = 1.8$ m/s), a problem that was solved in WISE 2001 by replacing the mechanical anemometer by an ultrasonic one, with an order-of-magnitude accuracy and resolution improvement.

As it will be discussed in Section IV, the results plotted in Fig. 13 are in agreement with [20] and [18] measurements, with reduced error bars. The following was found.

- Extrapolated sensitivity at nadir is estimated to be ~ 0.22 K/m/s).
- Sensitivity to WS increases at horizontal polarization, while decreases at vertical polarization.
- Around $\theta_i \sim 60°$, the brightness temperature at vertical polarization is insensitive to WS.

The fact that, at low incidence angles, the sensitivity of T_v to WS is larger than that of T_h—although within the error bars—is anomalous, since this behavior is not predicted by models, nor is present in Hollinger's [20] measurements. The point now is

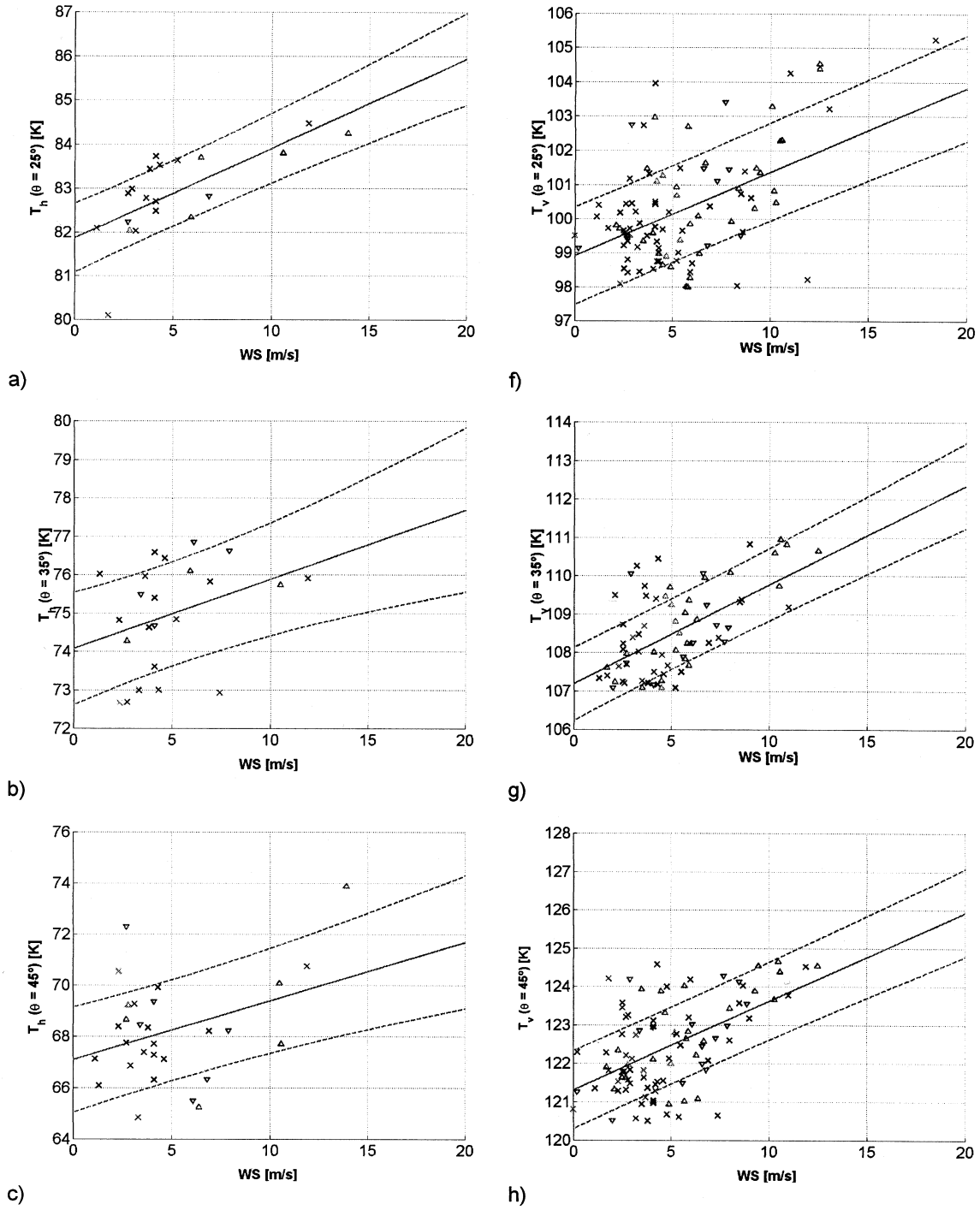

Fig. 12. Brightness temperature dependence with respect to wind speed of the L-band brightness temperature at horizontal (left) and vertical (right) polarizations at different incidence angles: (a) and (f) $\theta = 25°$, (b) and (g) $\theta = 35°$, and (c) and (h) $\theta = 45°$. Wind direction relative to radiometer: Δ = up-wind, ∇ = down-wind, $\times$ = cross-wind.

to try find out in WISE 2001 data if this phenomenon may be due to the presence of swell and/or by wave reflections on the platform structure (Section II-E, Fig. 2).

IV. Intercomparison With Numerical Models

The experimental results are compared with the Yueh two-scale model that has been recently found to compare well with brightness temperature measurements made at higher frequencies [11]. In its original form, it uses the wave spectrum in [22] multiplied by a factor of two. Since this factor was adjusted to fit measurements made at higher frequencies, comparisons were also performed using the Durden and Veseky spectrum and the more recent Elfouhaily spectrum [23]. This two-scale model has been implemented at LODYC (E. Dinnat, personnal communication) and has been run with the conditions (incidence angle, SSS, SST, WS, and direction) observed *in situ* during the radiometer measurements. Then, the simulated brightness temperatures were linearly fitted as a function of WS. This process

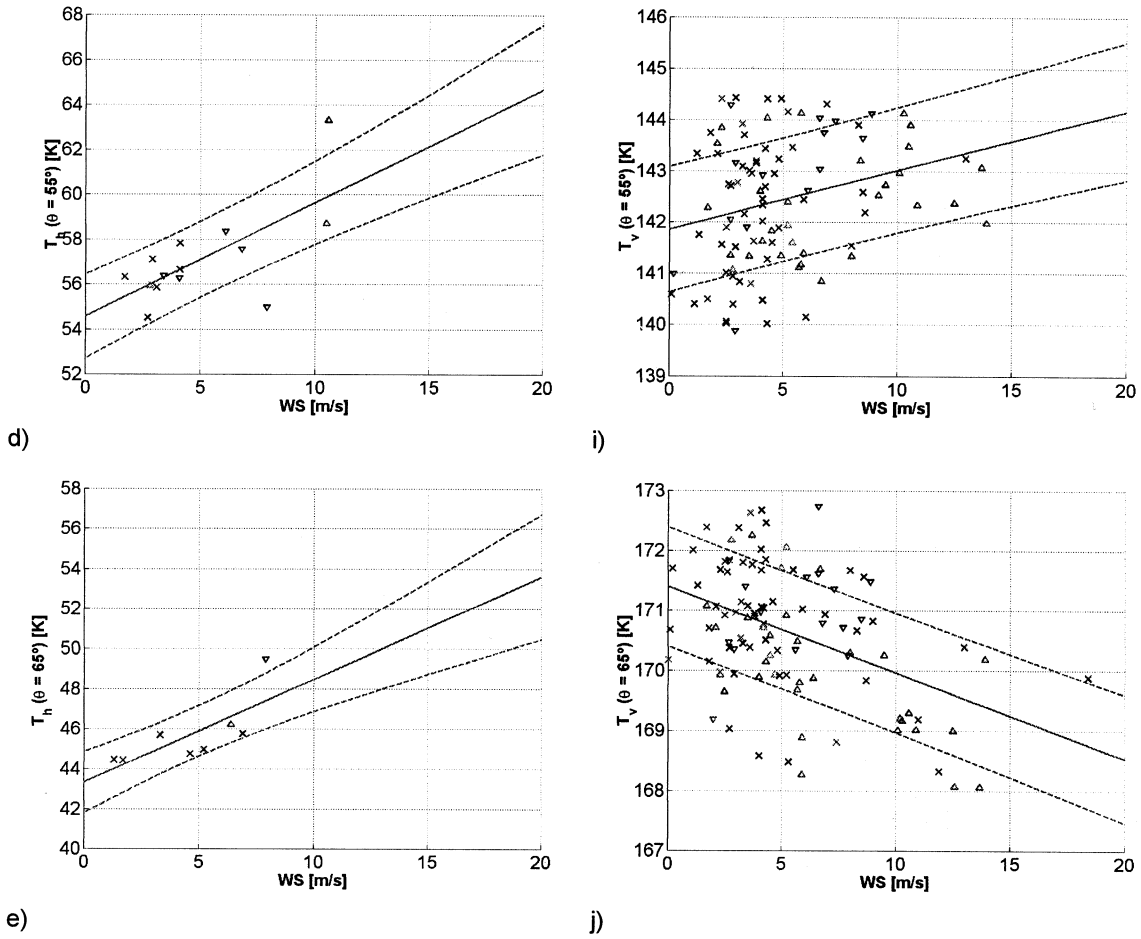

Fig. 12. *(Continued)* Brightness temperature dependence with respect to wind speed of the L-band brightness temperature at horizontal (left) and vertical (right) polarizations at different incidence angles: (d) and (i) $\theta = 55^\circ$ and (e) and (j) $\theta = 65^\circ$. Wind direction relative to radiometer: Δ = up-wind, ∇ = down-wind, $\times$ = cross-wind.

TABLE II
NUMBER OF DATA POINTS FOR EACH PLOT IN FIG. 12

	θ = 25°	θ = 35°	θ = 45°	θ = 55°	θ = 65°
H-polarization	20	23	29	14	8
V-polarization	100	74	98	102	100

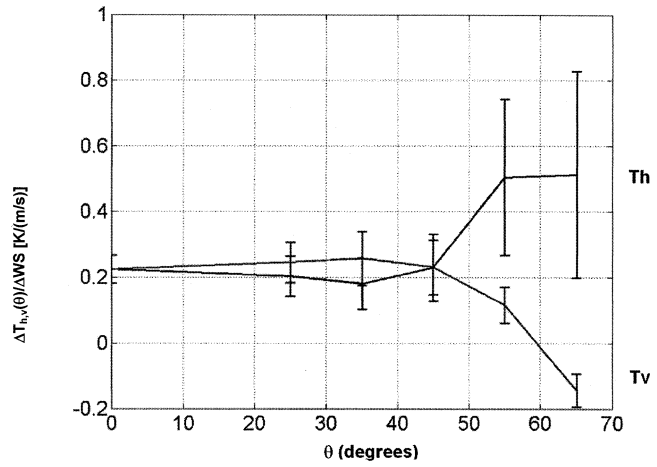

Fig. 13. Sensitivity of T_h and T_v to wind speed at 10-m height derived from Fig. 12.

has been performed for the three wave spectra: 1) Durden and Vesecky, 2) Elfouhaily, and 3) Durden and Vesecky multiplied by two (Fig. 14).

Results obtained with the Durden and Vesecky multiplied by two spectra (Fig. 14) appear to be close (most of the time inside the measurement's error bars) to the ones obtained from the *in situ* measurements (Fig. 13). However, further studies are required to better model possible disturbances of the wind/wave field due to the platform and due to limited fetch as well as foam effects that have been neglected.

Finally, Fig. 15 compares the WISE 2000-derived brightness temperature sensitivities (circles) to wind speed versus incidence angle at vertical and horizontal polarizations and comparison with Hollinger's measurements (diamonds) and Yueh–LODYC two-scale model (Durden–Vesecky spectrum multiplied by two, solid line).

As it can be appreciated, WISE 2000-derived sensitivities are in agreement with previously reported measurements within error bars. Even though the modeling results do not include foam, swell, or other effects, the comparison with the simulation results shows that the Durden and Vesecky spectrum multiplied by two provides closer results to the ones obtained from the *in situ* measurements than the results obtained with Durden and Vesecky or Elfouhaily spectra.

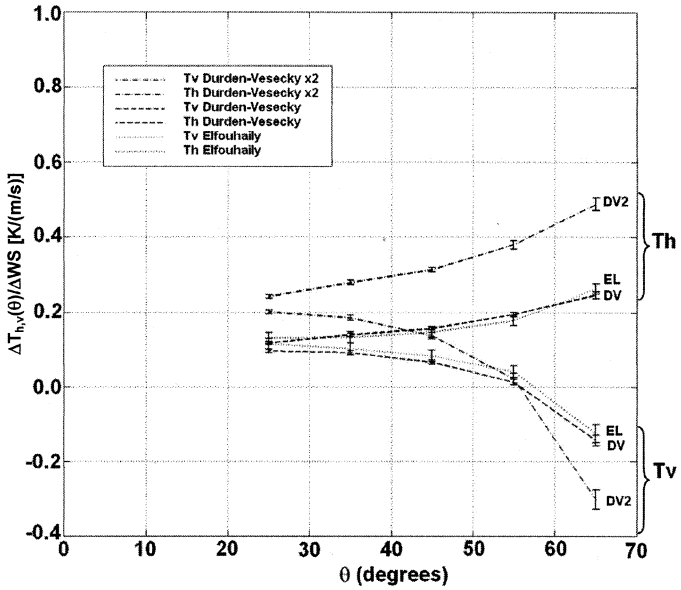

Fig. 14. Sensitivity of T_h and T_v to wind speed at 10-m height derived from Yueh–LODYC model with three different spectra.

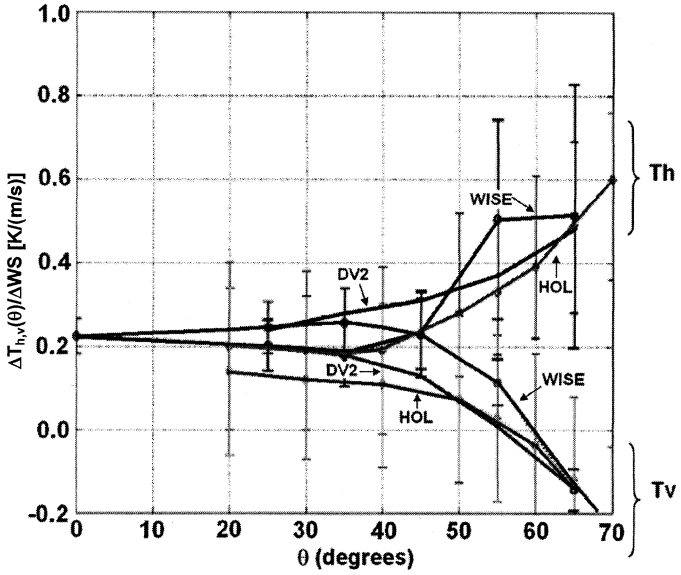

Fig. 15. WISE 2000-derived brightness temperature sensitivities to wind speed at 10-m height versus incidence angle at vertical (circles) and horizontal polarizations (circles) and comparison with Hollinger's measurements (diamonds) and Yueh–LODYC two-scale model (Durden–Vesecky spectrum x2, solid line).

Foam effects can be probably negligible below wind speeds smaller than 10 m/s. However, from the data, it is not easy to separate them, since most data points were acquired for wind speeds smaller than 10 m/s.

V. Conclusion

The Wind and Salinity Experiment 2000 has provided new data to better understand the effects of the wind in the emissivity of the sea at L-band. The experimental results confirm the existing experimental data with smaller associated error bars and should help improve the accuracy of the retrieval of SSS from airborne [24], [25] and spaceborne [26] radiometers.

The experimental results show a nadir sensitivity of 0.22 K/(m/s), increasing with incidence angle at horizontal polarization, and decreasing with incidence angle at vertical polarization, with a zero-crossing between 55° and 60°. The magnitude of the azimuthal variation of the first two Stokes parameters is on the order of 0.1–0.2 K approximately, although these results have to be confirmed by specific campaigns.

Numerical simulations performed with different spectra models indicate that the two-scale model using the Durden and Vesecky spectrum multiplied by two can be an appropriate description for the sea state. The analysis of the sea state reveals that most often the wind stress and the sea state are correlated, and the wind intensity and direction can be used to describe its state. However, in some situations, the correlation is quite low, meaning that the wave field originated somewhere else. In this case, further studies are required to characterize and model the swell.

The stereo-camera and video imagery results have corroborated the sea foam coverage dependence with wind speed for moderate water temperatures, although a large variability exists for the same wind conditions. An interesting point found was the lower foam coverage in the north side of the platform because of the stabilization of the incoming waves interfering with the reflected ones.

The retrieval of SSS from remote sensors requires the estimation of the WS and the SST. Even though the WS measurements from the buoy anemometer, the meteo station, and QUICKSCAT are in agreement ($\sigma_{\mathrm{WS\,meteo-WS\,buoy}} = 1.8$ m/s, $\langle \mathrm{WS_{meteo} - WS_{buoy}} \rangle = -0.9$ m/s, $\sigma_{\mathrm{WS\ meteo-WS\ Quickscat}} = 2.8$ m/s, $\langle \mathrm{WS_{meteo} - WS_{Quickscat}} \rangle = +0.4$ m/s), better absolute accuracy is required to use it as input parameter; otherwise the SSS-induced error becomes unacceptable ($\Delta T_{h,v}(\theta = 0^\circ)/\Delta \mathrm{WS} \approx 0.22$ K/m/s), $\Delta T_{h,v}(\theta = 0^\circ)/ = \Delta \mathrm{SSS} \approx 0.5$ K/psu at SST $= 20^\circ$ C). The IR SST estimates have proven to be accurate enough for the SSS retrieval process, exhibiting a small bias (~ -0.2 K) that increases at high incidence wind speeds, probably because of a lack of accurate modeling of the sea foam emissivity at the IR. Finally, the difference between -5 m and -20 cm salinity has been found to be smaller than 0.1 psu for most of the time, showing that SMOS calibration/validation measurements may be performed in most cases using standard -5 m salinity measurements.

Further research will be focused to 1) get more data points and better WS measurements so as to reduce the sensitivity to WS uncertainty, 2) study the sea state stability by looking at a series of brightness temperatures, and 3) determine the L-band emissivity of sea foam at different incidence angles to incorporate it in the numerical emission models.

Acknowledgment

The authors wish to thank S. Contardo for computational support at LODYC. They also thank Méteo-France for the help in the buoy data handling. Last, but not least, the authors very much appreciate all the cooperation and help provided by the personnel of Repsol Investigaciones Petrolíferas—Base Tarragona—Plataforma Casablanca for the organization of the campaign.

REFERENCES

[1] C. T. Swift and R. E. McIntosh, "Considerations for microwave remote sensing of ocean-surface salinity," *IEEE Trans. Geosci. Electron.*, vol. GE-21, no. 4, pp. 480–491, 1983.

[2] M. Martín-Neira and J. M. Goutoule, "A two-dimensional aperture-synthesis radiometer for soil moisture and ocean salinity observations," *ESA Bull.*, no. 92, pp. 95–104, Nov. 1997.

[3] P. Silvestrin, M. Berger, Y. Kerr, and J. Font, "ESA's second earth explorer opportunity mission: The soil moisture and ocean salinity mission—SMOS," *IEEE Geosci. Remote Sensing Newslett.*, Mar. 2001.

[4] S. D. Smith, "Coefficients for sea surface wind stress, heat flux, and wind profiles as a function of wind speed and temperature," *J. Geophys. Res.*, vol. 93, pp. 15 467–15 472, 1988.

[5] W. L. Smith, R. O. Knuteson, H. E. Revercomb, W. Feltz, H. B. Howell, W. P. Menzel, N. R. Nalli, O. Brown, J. Brown, P. Minnett, and W. McKeown, "Observation of the infrared radiative properties of the ocean—Implications for the measurement of the sea surface temperature via satellite remote sensing," *Bull. Amer. Meteorol. Soc.*, vol. 77, no. 1, pp. 41–50, 1996.

[6] P. D. Watts, M. R. Allen, and T. J. Nightingale, "Wind speed effects on sea surface emission and reflection for the along track scanning radiometer," *J. Atmos. Oceanic Technol.*, vol. 13, pp. 126–141, 1996.

[7] K. Masuda, T. Takashima, and Y. Takayama, "Emissivity of pure and sea waters for the model sea surface in the infrared window regions," *Remote Sens. Environ.*, vol. 48, pp. 302–308, 1988.

[8] C. J. Donlon and T. J. Nightingale, "Effect of atmospheric radiance errors in radiometric sea-surface skin temperature measurements," *Appl. Opt.*, vol. 39, no. 15, pp. 2387–2392, 2000.

[9] E. C. Monahan and M. Lu, "Acoustically relevant bubble assemblages and their dependence on metereological parameters," *IEEE J. Oceanic Eng.*, vol. 15, pp. 340–349, Oct. 1990.

[10] "Wind and Salinity Experiment-2000," ESTEC, Contract No 14 188/00/NL/DC, 2001.

[11] S. H. Yueh, W. J. Wilson, F. K. Li, S. V. Nghiem, and W. B. Ricketts, "Polarimetric brightness temperatures of the sea surface measured with aircraft K- and Ka-band radiometers," *IEEE Trans. Geosci. Remote Sensing*, vol. 35, pp. 1177–1187, Sept. 1997.

[12] A. J. Gasiewski and D. B. Kunkee, "Polarized microwave emission from water waves," *Radio Sci.*, vol. 29, no. 6, pp. 1449–1466, 1994.

[13] B. Laursen and N. Skou, "Wind direction over the ocean determined by an airborne, imaging, polarimetric radiometer system," *IEEE Trans. Geosci. Remote Sensing*, vol. 39, pp. 1547–1555, July 2001.

[14] A. Camps and S. C. Reising, "Wind direction azimuthal signature in the stokes emission vector from the ocean surface at microwave frequencies," *Microwave Opt. Technol. Lett.*, vol. 29, no. 6, pp. 426–432, June 2001.

[15] N. Reuil and B. Chapron, "Foam emissivity at L-band," ESTEC, WP1300 Rep., ESTEC Contract 15165/01/NL/SF, 2001.

[16] P. M. Smith, "The emissivity of sea foam at 19 and 37 GHz," *IEEE Trans. Geosci. Remote Sensing*, vol. 26, pp. 541–547, Sept. 1988.

[17] T. T. Wilheit, "A model for the microwave emissivity of the ocean's surface as a function of wind speed," *IEEE Trans. Geosci. Electron.*, vol. GE-17, no. 4, pp. 244–249, 1979.

[18] C. T. Swift, "Microwave radiometer measurements of the Cape Cod Canal," *Radio Sci.*, vol. 9, no. 7, pp. 641–653, 1974.

[19] H.-J. C. Blume, B. M. Kendall, and J. C. Fedors, "Measurement of ocean temperature and salinity via microwave radiometry," *Boundary-Layer Meteorol.*, vol. 13, pp. 295–308, 1978.

[20] J. P. Hollinger, "Passive microwave measurements of sea surface roughness," *IEEE Trans. Geosci. Electron.*, vol. GE-9, no. 3, pp. 165–169, 1971.

[21] S. H. Yueh, "Modeling of wind direction signals in polarimetric sea surface brightness temperatures," *IEEE Trans. Geosci. Remote Sensing*, vol. 35, pp. 1400–1418, Nov. 1997.

[22] S. L. Durden and J. F. Vesecky, "A physical radar cross-section model for a wind-driven sea with swell," *IEEE J. Oceanic Eng.*, vol. OE-10, pp. 445–451, 1985.

[23] T. Elfouhaily, B. Chapron, K. Katsaros, and D. Vandermark, "A unified directional spectrum for long and short wind-driven waves," *J. Geophys. Res.*, vol. 102, pp. 15 781–15 796, 1997.

[24] M. Goodberlet, C. T. Swift, K. P. Kiley, J. L. Miller, and J. B. Zaitzeff, "Microwave remote sensing of coastal zone salinity," *J. Coastal Res.*, vol. 13, no. 2, pp. 363–372, 1997.

[25] J. L. Miller, M. A. Goodberlet, and J. B. Zaitzeff, "Airborne salinity mapper makes debut in coastal zone," *EOS Trans.*, vol. 79, no. 14, pp. 173–177, Apr. 1998.

[26] M. Goodberlet and J. Miller, "NPOESS—Sea Surface Salinity," NOAA, Contract 43AANE704 017, 1997.

A. Camps (S'91–A'97–M'00) received the degree of Telecommunications Engineer and the Ph.D. degree in telecommunications engineering in 1992 and 1996, both from the Polytechnic University of Catalonia (UPC), Barcelona, Spain.

In 1991-1992, he received an Erasmus fellowship to study at the ENS des Télécommunications de Bretagne, France. In 1993, he joined the Electromagnetics and Photonics Engineering Group, Department of Signal Theory and Communications, UPC, as an Assistant Professor, and has been an Associate Professor since 1997. During 1999, he was on sabbatical leave at the Microwave Remote Sensing Laboratory, University of Massachusetts, Amherst. His research interest are focused on active and passive microwave remote sensing with special emphasis in aperture synthesis and interferometric radiometry (the European Space Agency's SMOS Earth Explorer mission).

Dr. Camps received the Second Spanish National Prize of University Studies in 1993, the INDRA award for the best Ph.D. in remote sensing in 1997, the UPC award for the best Ph.D. in 1999, the First Duran Farell Award for Technological Research (60.000 euros) along with the rest of the UPC radiometry team members, in 2000, and the City of Barcelona Award for Technological Research (8.000 euros) in 2001. In 2002, he received the Research Distinction of the Government of Catalonia for his contributions to passive microwave remote sensing. He is currently Associate Editor of *Radio Science* and the IEEE GEOSCIENCE AND REMOTE SENSING NEWSLETTER . He is also President of the Spanish Chapter of the IEEE Geoscience and Remote Sensing Society.

J. Font, photograph and biography not available at the time of publication.

J. Etcheto, photograph and biography not available at the time of publication.

V. Caselles, photograph and biography not available at the time of publication.

A. Weill, photograph and biography not available at the time of publication.

I. Corbella (M'99), photograph and biography not available at the time of tpublication.

M. Vall-llossera, photograph and biography not available at the time of publication.

N. Duffo (S'91–M'99), photograph and biography not available at the time of publication.

F. Torres, photograph and biography not available at the time of publication.

R. Villarino, photograph and biography not available at the time of publication.

L. Enrique, photograph and biography not available at the time of publication.

A. Julià, photograph and biography not available at the time of publication.

C. Gabarró, photograph and biography not available at the time of publication.

J. Boutin (A'01), photograph and biography not available at the time of publication.

E. Rubio, photograph and biography not available at the time of publication.

S. C. Reising (S'93–M'98), photograph and biography not available at the time of publication.

P. Wursteisen, photograph and biography not available at the time of publication.

M. Berger, photograph and biography not available at the time of publication.

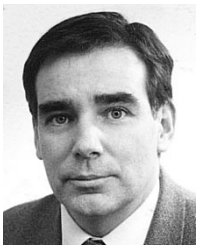

M. Martín-Neira (M'96) received the M.S. and Ph.D. degrees in telecommunication engineering in 1986 and 1996, respectively, from the School of Telecommunication Engineering, Polytechnical University of Catalonia, Catalonia, Spain.

From 1989 to 1992, he was was with GMV, a Spanish firm, where he was responsible for several projects for the European Space Agency (ESA) related to global positioning satellite navigation with applications to precise landing and attitude determination. Since 1992, with ESA, he has been in charge of the radiometer activities within the Payload, Equipment, and Technology Section. During this period, he has been responsible for the technology activities related to the Microwave Imaging Radiometer with Aperture Synthesis (MIRAS) project.

Dr. Martín-Neira was awarded a Fellowship to work on radiometry at European Space Research and Technology Center (ESTEC), Noordwijk, The Netherlands, in 1988.